Formation of Silicon Nanoclusters in Disproportionation of Silicon Monoxide

D. A. Lozhkina[a],*, E. V. Astrova[a], R. V. Sokolov[a], D. A. Kirilenko[a], A. A. Levin[a], A. V. Parfeneva[a], and V. P. Ulin[a]

[a] Ioffe Institute, St. Petersburg, 194021 Russia
*e-mail: darina.lozhka94@gmail.com

Abstract—The processes of the disproportionation of solid-phase silicon monoxide, accompanied by the formation of nanocrystalline silicon precipitates in the medium of amorphous suboxide SiO_x (initial composition of $SiO_{0.9}$), are studied. Based on the data of X-ray diffraction analysis and transmission electron microscopy, the dynamics of changes in the amount, concentration, and size of phase precipitates of silicon with the temperature of isochronous annealing increasing from 800 to 1200°C is traced. It is found that, with the total mass of the precipitated silicon steadily increasing, the number of its crystallization centers per unit volume nonmonotonically depends on temperature. The activation energy of the diffusion of silicon atoms in the SiO_x matrix is determined to be $E_{a1} = 1.64$ eV and the activation energy of their transfer from precipitates formed to the SiO_x growth medium is $E_{a2} = 2.38$ eV. The anisotropic deformation of silicon crystallites precipitated during the disproportionation of SiO is revealed for the first time. This phenomenon is attributed to the difference between the specific volumes of the phases being separated and to the anisotropy of the growth rate of silicon precipitates formed in a solid amorphous medium.

1. INTRODUCTION

Solid-phase silicon monoxide is a product of fast condensation on a cold surface of SiO molecules, which appear in the gas phase upon the high-temperature (1250–1400°C) reduction of SiO_2 with silicon, and also in such nonequilibrium processes as the reactive sputtering of silicon or the plasma-chemical oxidation of silanes. Condensed silicon monoxide is amorphous and exists in the metastable state in relation to decomposition into the thermodynamically stable phases of silicon and silicon dioxide. However, the high strength of the chemical bonds Si–O (bond energy $E = 3.82$ eV) and Si–Si ($E = 1.82$ eV) results in that the "frozen" state of the structure, which arises during the nonequilibrium condensation of molecules, remains unchanged nearly in the whole range of temperatures required for the operation of electronic and optical devices. This enables the wide use of SiO films as dielectric layers in electronics and antireflection coatings in optics. At the same time, the stage-by-stage decomposition of SiO into stable phases, which occurs at substantially higher temperatures, opens up prospects for the simple synthesis of composite materials with crystalline-silicon clusters of controlled size, fixed in an amorphous dielectric medium. Materials of this kind, which are in various disproportionation

stages, are of particular interest in both scientific and application regards: from objects for the study of quantum-confinement effects in nanoparticles [1, 2] to their use as electrode components of lithium-ion batteries [3].

The nature of short-range ordering of the structure in amorphous silicon monoxide had long remained under discussion, but it has been found recently with sufficient definiteness that all silicon atoms in the structure of SiO are in the sp^3-hybrid state and tend to acquire a tetrahedral environment [4, 5]. Accordingly, amorphous silicon monoxide SiO must be constructed from five kinds of adjustable structural units $Si(Si_{4-y}O_y)$, where y can take values in the range from 0 to 4. The existing composite models of SiO allow various quantitative relationships between units forming the structure and, accordingly, various depths of SiO disproportionation, recorded at the instant of formation of the solid phase. In accordance with the random-mixture (RM) model [6, 7], SiO is predominantly constituted by units of two types, $Si(Si_4)$ and $Si(O_4)$, which corresponds to silicon and silicon dioxide phases. In this case, silicon forms nanoscale clusters randomly distributed in an amorphous matrix. Another model of random bonding (RB) [8] assumes a statistical distribution of all kinds of units. In the

opinion of the authors of [4] the most probable is the model in which Si and SiO_2 regions with diameter of 0.5–2.5 nm are connected by interphase transition layers constituted by $Si(Si_{4-y}O_y)$ units ($y = 1-3$), with the volume fraction of a suboxide of this kind in the total volume of the material being < 25%. The formation of the transition regions was considered in detail in [9] and was experimentally confirmed in [10].

The reaction of SiO disproportionation

$$2SiO = Si + SiO_2 \qquad (1)$$
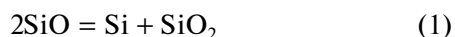
has long been known in the chemistry of silicon and is used as a simple method for obtaining silicon nanoparticles. However, the mechanism of Si/SiO_2 phase separation in the high-temperature annealing of SiO remains incompletely understood. The difference between the methods and conditions for the precipitation of silicon monoxide and SiO_x suboxides close to it in composition give rise to the initial dissimilarity of short-range order structures in these materials. It is likely that this is why numerous studies of the kinetics of their disproportionation, performed on both bulk and film samples, have demonstrated a significant scatter of the values obtained for the activation energies of the diffusion of silicon and growth of its precipitates [11–15]. The most important task for practical applications, such as anodes of Li-ion batteries, is to control the size and concentration of silicon precipitates formed in the oxide as a result of disproportionation of the initial material.

In the present study, we examine by quantitative X-ray phase analysis and transmission electron microscopy the specific features of how silicon nanoclusters are formed in bulk silicon monoxide subjected to isochronous annealing at various temperatures.

2. EXPERIMENTAL

As the initial material served the domestic commercial product SiO of special-purity grade, ground in an agate mortar and subjected to heat treatment in the temperature range 800–1200°C. Some samples were annealed at a higher temperature of 1225°C. Annealing was performed in a muffle furnace with a horizontal quartz tube blown-through with high-purity argon [99.998%, TU (Technical specification) 6-21-12-94. The content of impurities in Ar: $[O_2] < 2 \times 10^{-4}\%$, $[H_2O] < 3 \times 10^{-4}\%$]. The silicon-monoxide powder was placed in a quartz boat, moved into the working zone of the furnace, and kept there for 1 h.

The X-ray diffraction measurements of the initial SiO and the monoxide subjected to disproportionation were performed with a D2 Phaser powder diffractometer (Bruker AXS, Germany). Emission from an X-ray tube with a copper anode, monochromatized with a Ni filter (CuK_α radiation), was used. The X-ray diffraction (XRD) patterns were recorded with a LYNXEYE semiconductor linear position-sensitive

X-ray detector (PSD, Bruker AXS, Germany) with an aperture angle of 5°. Measurements were made in the $\theta-2\theta$ symmetry scanning mode in the vertical Bragg–Brentano configuration $\theta-\theta$. The diffraction patterns were recorded via multiple scanning of the interval $2\theta = 5-120°$ with a step of $\Delta 2\theta = 0.02°$ and intensity-accumulation time at a point of 1 s. In the case of the linear PSD used in the study, this corresponds to an effective time of 165 s of the point detector being stationary at every step. The total effective time of intensity accumulation at a point was 1320 s. The temperature in the chamber in which the sample was placed was, during the measurements, 41.3°C. To reduce the effect of the possible predominant orientation of crystallites, the sample was rotated during measurements about the holder axis, which coincided with that of the axis of the goniometer of the diffractometer. To correct the diffraction patterns for the shift of the counter to zero ($\Delta 2\theta_{zero}$) and correct the angular positions of reflections for the shift because of possibly missing the focal plane ($\Delta 2\theta_{displ}$), a NaCl powder was added to the samples under study (1.25 wt %). This powder was preliminarily calibrated against the X-ray powder standard Si640d (NIST, USA). X-ray phase analysis of the diffraction patterns was performed using the EVA software (Bruker AXS, Germany) with the following databases: powder diffraction file-2 database (PDF-2, ICDD, 2014) and crystallographic open database (COD) [17], as well as published data for silicon monoxide [18–21].

It is impossible to correctly determine the mass content both of nanocrystalline phases and of silicon monoxide by the Rietveld method because SiO does not exist in the crystalline state and its structure (atomic coordinates, unit-cell parameters, and space group) is unknown. Therefore, the experimental diffraction patterns with strongly superimposed reflections were decomposed into separate reflections by Fityk software [22]. To carry out further analysis with this program, a correction was made for the contribution from the background and the following reflection parameters were obtained: Bragg angle 2θ, the full width of the reflection at half maximum (FWHM), and its integrated and maximum intensities. The SiO reflection peaked at $2\theta \approx 22°$ was approximated with a LogNormal function, and the remaining reflections, by the Pearson 7 function. This choice of functions provided a better agreement with the experiment, than the Lorentzian function used in [14].

The absolute values of the content of silicon in the annealed SiO samples were determined for each annealing temperature by scaling with respect to the amount of Si in the initial material. The weight fraction of Si in the initial SiO was found by analysis of the X-ray diffraction patterns of the samples, to which different amounts of silicon nanopowder (nano-Si) were added. The diameter of the crystalline particles of the powder being added was 30–50 nm (commercial

product from Hongwu Nanometer). A preliminary analysis of the diffraction patterns confirmed that the reference powder corresponds in peak positions and intensities to nanocrystalline silicon with a particle size of ~40 nm. The fact that this reference material was chosen indicates that, in performing a quantitative X-ray diffraction analysis in the given case, the systematic inaccuracy in determining the X-ray reflection parameters is insignificant because of the difference in the absorption factor and phase textures. In this case, the reflections associated with the added nano-Si are substantially narrower than those associated with particles of silicon precipitates, which enables their reliable separation in the analysis of a diffraction pattern.

The size of the coherent-scattering region (*D*, size of crystallites) was found from the reflection widths by the Selyakov−Scherrer formula:

$$D = K\lambda/(\beta\cos\theta),$$

where *D* is the size of crystallites in nm; λ is the radiation wavelength, 0.154 nm in our case; θ is the scattering angle (half the diffraction angle 2θ); and β is the physical broadening of the line in the diffraction pattern (FWHM) in radians. For simplicity, the coefficient *K* was taken in the present study to be unity. Because the observed reflections are wide (the FWHM of the reflections substantially exceeds their instrumental broadening) the instrumental broadening was neglected in the calculations. The size of Si nanocrystallites was found as the average of the values obtained for three Si reflections: 111, 220, and 311.

The measurements by transmission electron microscopy (TEM) were performed with a Jeol JEM-2100F microscope (accelerating voltage 200 kV, point resolution 0.19 nm). The material was deposited in the form of a powder onto ultrathin amorphous-carbon films supported by a copper grid. The study was carried out with the use of methods of electron diffraction, diffraction contrast, and high-resolution transmission electron microscopy. Dark-field images of silicon and silicon-oxide nanoclusters were obtained in the appropriate position of the objective aperture in the plane in which the electron diffraction pattern was formed.

3. EXPERIMENTAL RESULTS

3.1. X-Ray Diffraction Analysis

Figure 1 shows the experimental X-ray diffraction patterns of a SiO powder annealed at different temperatures. Silicon monoxide gives broad reflections that are characteristic of the amorphous state [5] and are peaked near $2\theta = 22°$, 50°, and 69° (the portion with the last of the reflections is not shown). In the part of the diffraction pattern shown in the figure, the silicon reflections 111, 220, and 311 also can be seen. As the annealing temperature is raised to more than
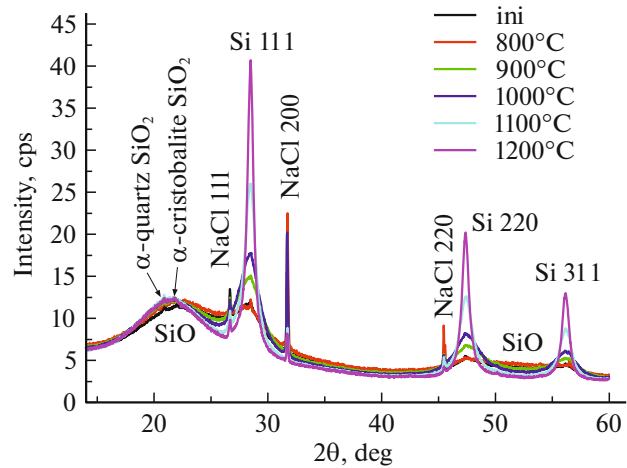

Fig. 1. Part of the diffraction pattern of silicon monoxide annealed at different temperatures (ini designates the initial, thermally untreated material). A crystalline NaCl powder is added for calibration purposes to the powders of silicon monoxide after annealing.

800°C, their intensity grows and the FWHM decreases. In addition, the diffraction patterns have at 21° and 22° low-intensity reflections from various modifications of crystalline silicon dioxide SiO_2.

3.2. Transmission Electron Microscopy

The main structural differences between the initial sample and that annealed at a high temperature are presented in Fig. 2. The electron diffraction pattern of the initial material (Fig. 2a) shows rings of nanocrystalline Si and a halo of nanocrystalline SiO_2 and amorphous Si monoxide. After high-temperature annealing, point-like diffraction reflections appear in the electron diffraction patterns (Fig. 2b), which indicates that silicon clusters become coarser. This is also confirmed by high-resolution images (Figs. 2c and 2d) after annealing, crystalline particles are well seen in the amorphous matrix. The interplanar spacings in these particles correspond to the {111} planes of silicon.

Figures 2e and 2f also clearly demonstrate that high-temperature treatment also results in that the size of the silicon particles noticeably increases, as also does the average distance between these particles. At the same time, SiO_2 nanoclusters do not undergo noticeable changes (Figs. 2g and 2h).

4. ANALYSIS AND DISCUSSION OF RESULTS

4.1. Decomposition of the Experimental Diffraction Patterns into Separate Reflections

Similarly to other authors who examined silicon monoxide by means of X-ray diffraction analysis [18−21], we observe in the initial material broad SiO
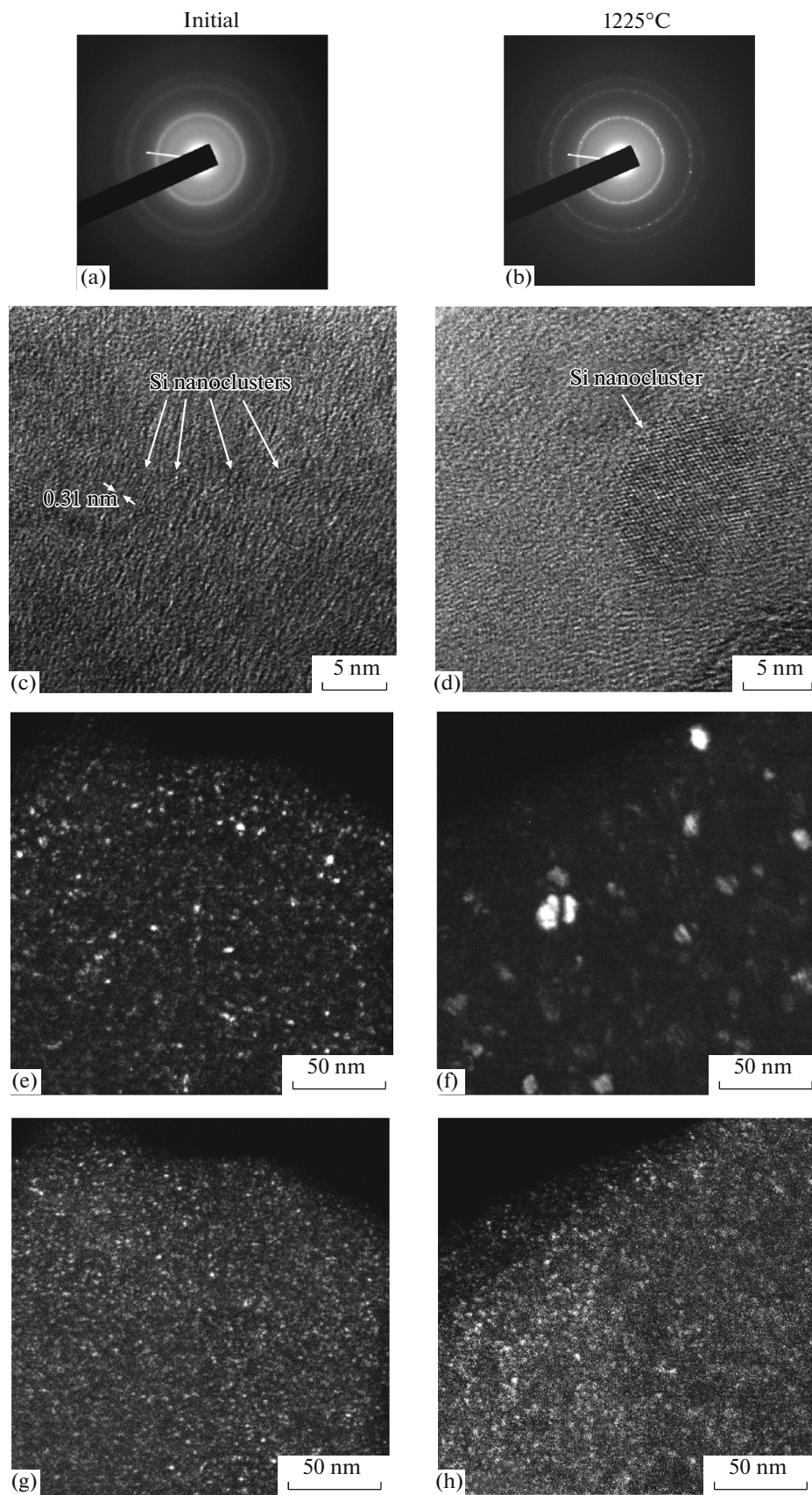
Initial   1225°C

Fig. 2. Comparison of samples of the initial SiO (left column, a, c, e, g) and annealed at 1225°C (right column, b, d, f, h) on the basis of TEM data: (a, b) electron diffraction patterns, (c, d) High-resolution electron-microscopic (HREM) images, (e, f) dark-field images of silicon nanoclusters, (g, h) dark-field images of silicon-oxide nanoclusters.
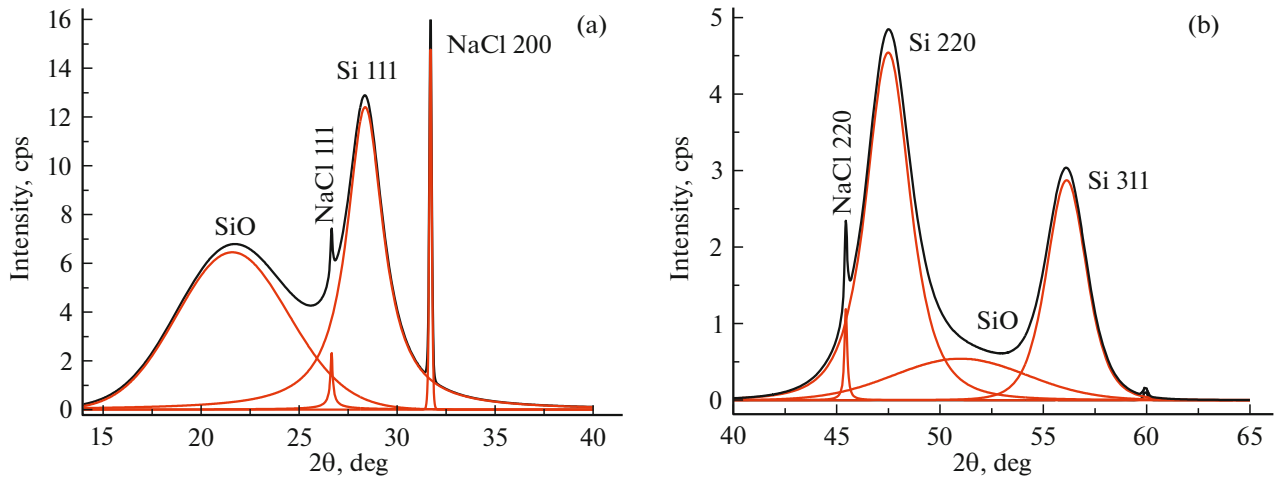
Fig. 3. Decomposition into the constituent reflections of the diffraction pattern of the sample annealed at $T = 1000°C$ with the addition of a crystalline NaCl powder. Ranges of reflection angles: (a) $2\theta = 14°-40°$ and (b) $40°-65°$.

reflections, which change with increasing annealing temperature. The intensity of the first SiO reflection (peaked at $2\theta \approx 22°$) grows with increasing temperature, and the peak itself shifts to smaller 2θ angles (Fig. 4a) thereby approaching the angular position of the reflection of cristobalite with $hkl = 101$ (PDF card 00−039−1425). This effect of the phase separation into Si and SiO_2, in which the tetrahedra of the initial material $Si(Si_{4-y}O_y)$ ($y = 1-3$) are gradually converted into Si−O_4 and Si−Si_4 tetrahedra was also observed in [14]. To our knowledge, the behavior of the second SiO reflection ($2\theta \approx 52°$) has not been analyzed in publications so far. It appeared that, compared with the first reflection, it is more sensitive to the annealing temperature: with this temperature increasing, the maximum intensity of the reflection noticeably decreases and the reflection is more strongly shifted to smaller angles (Fig. 5). The third reflection at $2\theta \approx 69°$ has a low intensity and overlaps with the silicon reflection $hkl = 400$, which hinders its analysis.

Let us analyze the reflections associated with silicon. It can be seen in Fig. 1 that the initial monoxide SiO already contains phase precipitations of silicon, the presence of which in unannealed samples has also been noted by other authors [13]. The integrated intensity A of the corresponding reflections grows, beginning at 800°C, which coincides with the temperature at which [5] first indications of the separation of SiO into individual phases is observed.

It can be seen in Table 1 that annealing at 1200°C leads to a nearly 5-fold increase in the amount of the silicon phase (columns $A28/m$, $A47/m$, $A56/m$). To find from the diffraction patterns in Fig. 1 the absolute values of the content of Si in the annealed samples, we estimated the amount of Si in the initial SiO. For this purpose, we measured the diffraction patterns of the initial silicon monoxide with the addition of a certain amount of silicon nanopowder (1.25, 2.5, 3.75 wt %).

It can be seen in Fig. 6 that the X-ray diffraction patterns are well superimposed, with differences only observed in a narrow range of angles in the region of the silicon peaks. It is noteworthy that a gradual

Table 1. Integrated intensities of Si reflections (A) in relation to the annealing temperature (T) of SiO samples

T, °C	m, * mg	$A28$**	$A47$**	$A56$**	$A28/m$***	$A47/m$***	$A56/m$***
ini	195.1	9.5	5.5	2.4	4.9	2.8	1.2
800	150.4	8.6	8.5	2.5	5.7	5.6	1.7
900	158.0	17.4	14.0	5.8	11.0	8.9	3.7
1000	143.1	22.9	13.3	7.9	16.0	9.3	5.5
1100	157.8	26.8	17.7	9.8	17.0	11.2	6.2
1200	136.7	29.7	17.4	10.6	21.7	12.7	7.8

* m is the mass of the SiO powder used in the experiment. ** $A28$, $A47$, and $A56$ are the integrated intensities (in cps deg) of, respectively, Si reflections 111 ($2\theta \approx 28.4°$), 220 ($2\theta \approx 47.3°$), and 311 ($2\theta \approx 56.1°$) for the Si phase, obtained be decomposition of the diffraction patterns (Fig. 1) upon their being corrected with consideration for the contribution of the background. *** $A28/m$, $A47/m$, and $A56/m$ are the integrated intensities **, but normalized to the mass m.
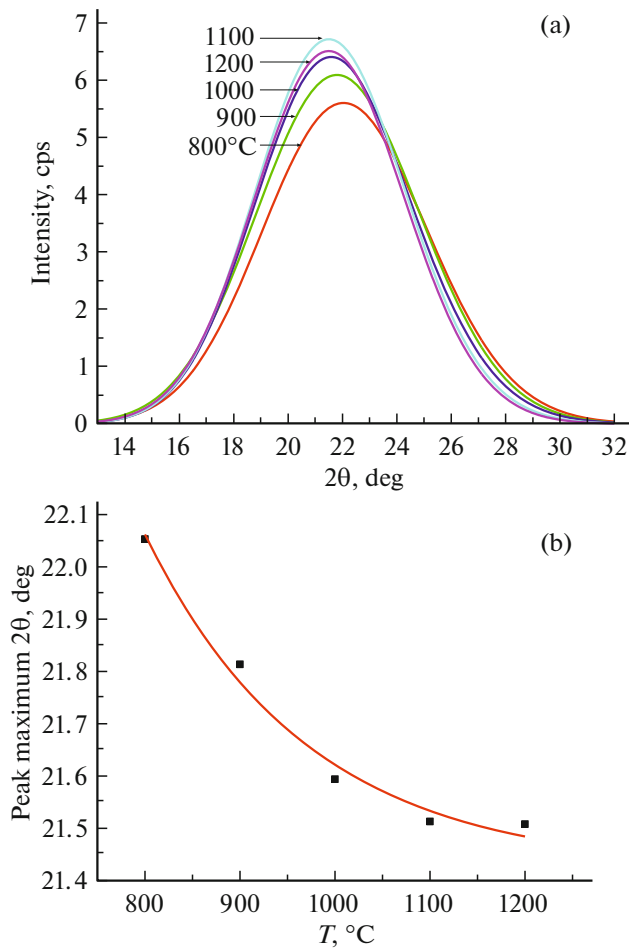
Fig. 4. (a) Variation in the shape of the first SiO reflection and (b) shift of its peak with the heat-treatment temperature.

Fig. 5. (a) Variation with temperature of the shape of the second SiO reflection and (b) shift of its peak at high annealing temperatures.

increase in the amount of nanocrystalline silicon does not change the diffraction patterns at angles we attributed to the SiO range in Figs. 1 and 3. This fact makes it possible to relate changes in the diffraction patterns, seen in Fig. 1, exclusively to the processes of SiO disproportionation in the course of annealing of the samples. An example of good separation of the rather narrow reflections from nano-Si and broad reflections from Si produced via the disproportionation of SiO is presented in Fig. 7 (reflections with integrated intensities A_n and A_w, respectively). The ratio between the integrated intensities of these reflections, A_w/A_n, and the known mass of added silicon powder, p_0, were used to determine the amount of Si in the initial material $i = p_0 A_w/A_n$. The values obtained for the concentration of silicon in the initial material, found for different reflections, are listed in Table 2.

It can be seen in Fig. 7 and Table 2 that the integrated intensity of the wide peaks of silicon remains approximately the same for samples with different amounts of added Si nanopowder. Thus, upon averag-
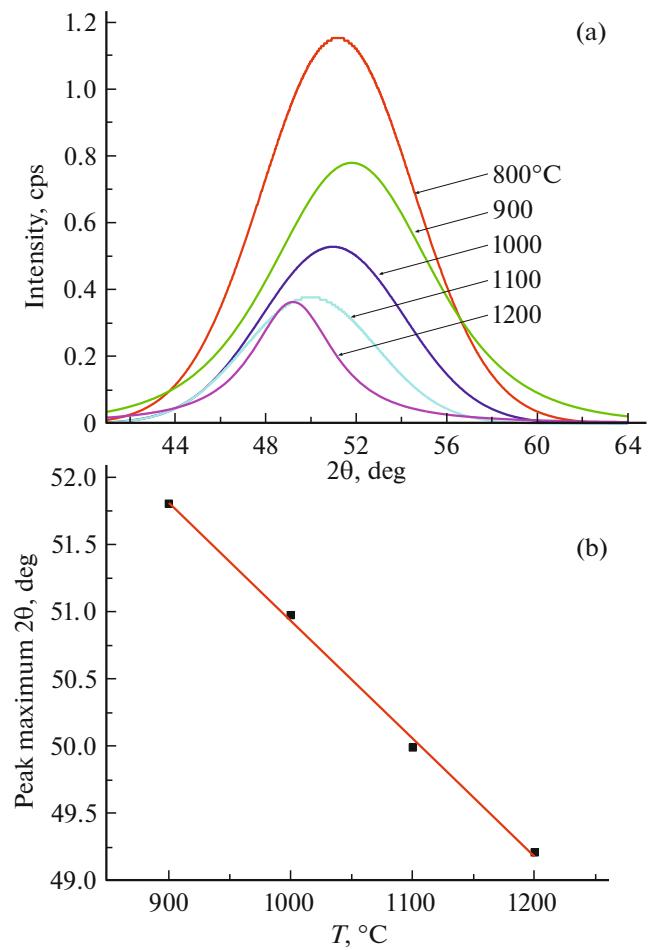
ing, the content of crystalline Si in the initial material can be estimated at 6.7 wt %, and, knowing this content, we can determine the absolute values of the content of silicon p (in wt %) in the samples subjected to annealing. The calculation was based on the data in Table 1 for three reflections: $p(28) = (6.7/4.9)$ $(A28/m)$, $p(47) = (6.7/2.8)$ $(A47/m)$, $p(56) = (6.7/1.2)$ $(A56/m)$. The resulting percentage content of the silicon phase formed is presented in Table 3.

Figure 8 shows how the average concentration of the precipitated Si, p_{av}, found for three reflections, varies with increasing SiO annealing temperature.

It follows from the equation of the disproportionation reaction (1) that, if the initial material has a stoichiometric composition, it contains 50 at % of elementary Si. If full conversion occurs in this material, with the whole amount of SiO decomposing into Si and SiO_2, the Si content of interest in the resulting material is 25 at %. Recalculated to the mass content, this gives 31.8%. Thus, this is the maximum amount of Si that can be formed in accordance with the reaction
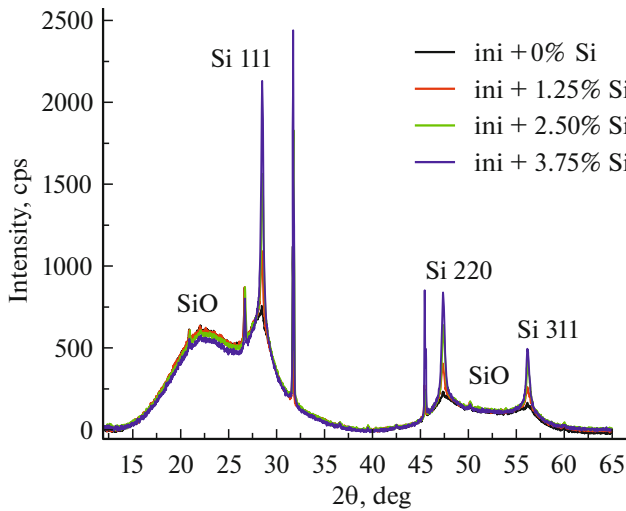
Fig. 6. Diffraction patterns of samples of the initial SiO with varied content of Si nanopowder after the correction for background contributions.
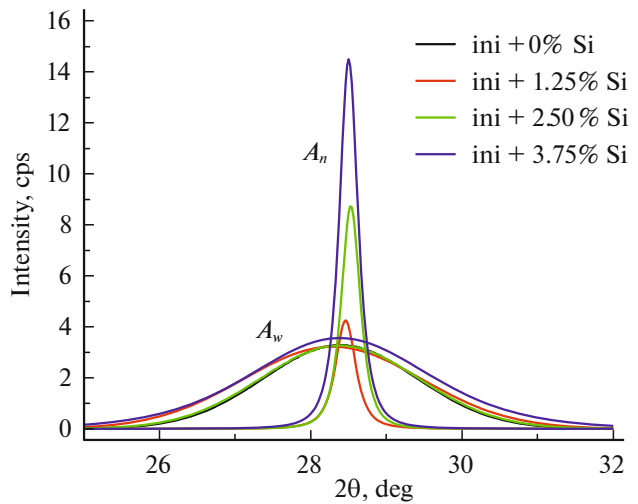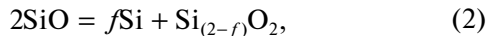

Fig. 7. Contributions to the intensity of the Si 111 reflection, obtained from the initial SiO material (wide reflections with the integrated intensity A_w) and from the nanodisperse silicon powder added to the samples (narrow reflections with the integrated intensity A_n).

of disproportionation of silicon monoxide of stoichiometric composition. For our material, the limiting concentration of silicon nanocrystals is, with consideration for the initial amount present, 6.7% higher and constitutes 38.5%.

Thus, the main phases in the samples under study before and after annealing are the X-ray-amorphous SiO_x phase (with various values of x) and nanocrystalline Si. Also present is a small number of nanocrystalline phases of silicon dioxide SiO_2: cristobalite, quartz and, after annealing at 1225°C, tridymite.

4.2. Composition of the Matrix

Let us consider the partial disproportionation of silicon monoxide SiO_x of stoichiometric composition ($x = 1$). Let us designate by f the number of atoms of precipitated Si. Then

$$2SiO = fSi + Si_{(2-f)}O_2, \qquad (2)$$

$$x = 1/(1 - 0.5f). \qquad (3)$$

Taking into account the molecular and atomic masses

$$p_s = (28f/88) \times 100\% = 31.8f, \qquad (4)$$

where p_s is the mass fraction in % of the silicon phase that appears as a result of the disproportionation of SiO of stoichiometric composition. Hence follows that

$$x = 1/[1 - 0.0157p_s]. \qquad (5)$$

Figure 9 shows how the average composition of the remaining silicon suboxide depends on the amount of precipitated silicon. It can be seen that x grows from 1 to 2 when f varies from 0 to 1 (or, in mass fractions of Si from 0 to 31.8%).

Analysis of the X-ray diffraction patterns shows that the material under study initially contains a certain amount of silicon nanoparticles as a separate

Table 2. Integrated intensities of the wide and narrow silicon peaks into which are decomposed three different reflections of silicon in the initial SiO with different amounts of added nano-Si

p_0, %	$Aw28$ wide	$An28$ narrow	$Aw47$ wide	$An47$ narrow	$Aw56$ wide	$An56$ narrow	$i28$, %	$i47$, %	$i56$, %	$i_{av}(28{-}56)$, %
0	9.5	0	5.5	0	2.4	0	—	—	—	—
1.25	10.5	1.7	5.0	1.3	3.5	0.9	7.7	4.9	4.9	→5.8
2.50	9.2	3.2	5.9	2.4	3.4	1.0	7.2	6.1	8.5	→7.3
3.75	11.1	5.4	5.6	2.9	2.9	1.7	7.7	7.2	6.4	→7.1
										Average over three values of p_0: $i = 6.7$

$A28$, $A47$, and $A56$ are the integrated intensities (in cps deg) of, respectively, Si reflections 111 ($2\theta \approx 28.4°$), 220 ($2\theta \approx 47.3°$), and 311 ($2\theta \approx 56.1°$) for the nano-Si phase (narrow) and the Si phase (wide) of a SiO sample in the diffraction patterns of the samples to which nano-Si powder was added (Fig. 6). $i28$, $i47$, and $i56$ are the amounts of Si in the initial SiO sample, estimated from Si reflections 111, 220, and 311, respectively.
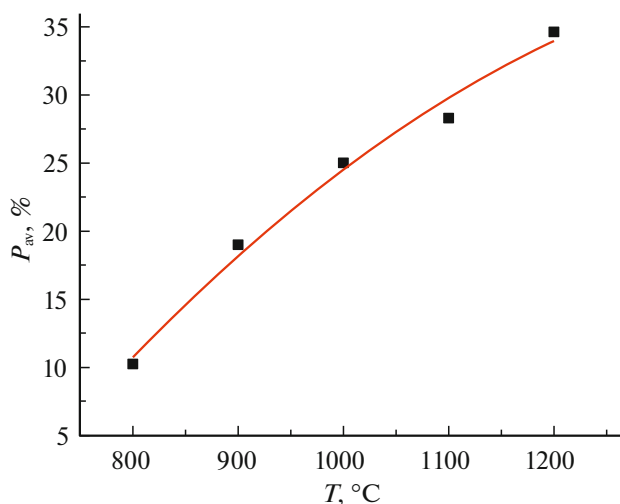
Table 3. Percentage content of the silicon phase relative to the SiO annealing temperature according to the data for three reflections (111, 220, and 311) and the calculated composition of the SiO_x suboxide matrix being formed (see Section 3.3)

T, °C	$p(28)$, %	$p(47)$, %	$p(56)$, %	p_{av}, %Si average	x in SiO_x matrix
ini	6.7	6.7	6.7	6.7	1.0
800	7.8	13.5	9.5	10.3	1.1
900	15.1	21.3	20.6	19.0	1.2
1000	21.9	22.3	30.8	25.0	1.4
1100	23.3	26.9	34.7	28.3	1.5
1200	29.7	30.5	43.7	34.6	1.8

phase. In all probability, these nanoparticles were not formed as a result of the disproportionation of SiO proper, but appeared already in the stage of condensation of the gas-phase components in the course of the association of silicon atoms that are in excess with respect to oxygen. Then, assuming that the initial material is a mixture of stoichiometric SiO and excess silicon with the atomic fraction z, we can represent its composition by the general formula $Si_{(1 + z)}O$. Based on the fact that the excess of Si is 6.7% according to our estimate, z can be found from the equation

$$28z/[28(z + 1) + 16] = 0.067, \quad (6)$$

where 28 is the atomic mass of Si, and 16 is that of oxygen. Hence follows that $z = 0.11$ and, accordingly, the chemical formula of the material under study can be written as $Si_{1.11}O$ or $SiO_{0.9}$. As silicon precipitates are formed, the composition of the surrounding matrix is shifted from SiO toward a larger content of oxygen. The temperature dependence of the composition of the remaining suboxide SiO_x can be determined using the above values of p (Table 3), from which, to find p_s, it is necessary to subtract $i = 6.7\%$, $p_s = p - i$ and then find x by formula (5). The related results are presented in the last column of Table 3, whence it can be seen that no complete transformation of the oxide matrix into SiO_2 occurs even at the highest annealing temperature in our experiment (1200°C).

4.3. Size and Concentration of Silicon Precipitates

The sizes of Si crystallites at different annealing temperatures, calculated from different X-ray reflections by the Selyakov−Scherrer formula and then averaged, are presented in Fig. 10 and Table 4. The dependence in Fig. 10 shows that the growth of precipitates occurs with increasing temperature by a nearly exponential law.

The data obtained on the amount of the Si phase and size of precipitates can be used to estimate the variation of their number with temperature. Assuming that Si crystallites are spherical with the diameter D, we find the average values of the volume and mass of a particle: V_p and m_p. Assuming that the total density of the annealed samples is invariable (2.13 g/cm³) and knowing the mass content of the silicon precipitates

Fig. 8. Amount of silicon formed in SiO disproportionation in relation to the annealing temperature.
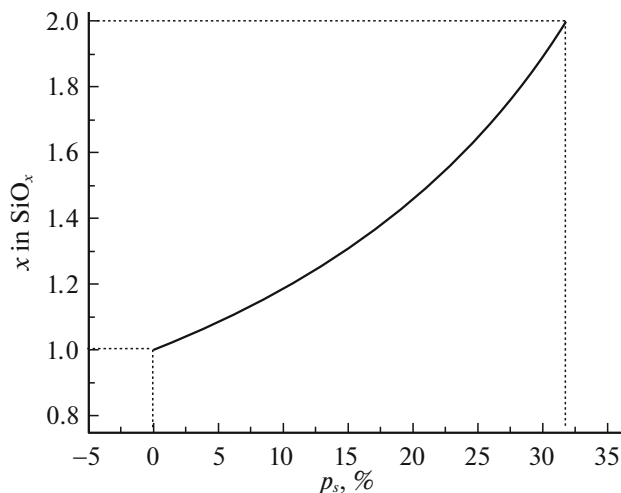
Fig. 9. Calculated dependence of the composition of the SiO_x amorphous matrix on the amount p_s of crystalline silicon precipitated in the disproportionation of SiO with a stoichiometric composition.
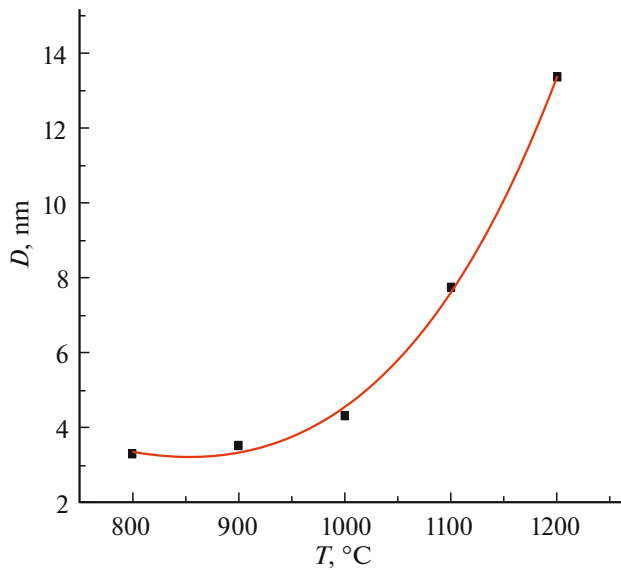
Fig. 10. Variation in the average size of Si crystallites with increasing SiO disproportionation temperature according to the results of X-ray diffraction analyses.

Fig. 11. Variation in the concentration of silicon precipitates with the SiO annealing temperature.

(p_{av} in Table 3), we determine the mass of silicon M_{Si} in 1 cm³ of the matrix and then find the number of silicon precipitation centers, $N = M_{Si}/m_p$; volume per center, v; and the average distance between the centers, L. The values obtained are listed in Table 4.

Figure 11 presents the dependence of the number N of crystallization centers in a unit volume of the material on the heat-treatment temperature. It can be seen in Table 4 and Fig. 11 that, up to $T \approx 900°C$, raising the temperature of SiO annealing leads to an increase in the concentration of the silicon phase nuclei dispersed in the oxide phase. However, beginning at 900°C, their concentration decreases against the background of a rather sharp increase in the size of the clusters being formed. This result agrees with the data of [12], in which it was found that making the annealing longer at $T = 900°C$ results in that the number of precipitates grows without changes in their size. This dependence shows that, at comparatively low temperatures, the segregation of silicon atoms, accompanying the processes of the transformation of mutually related struc-
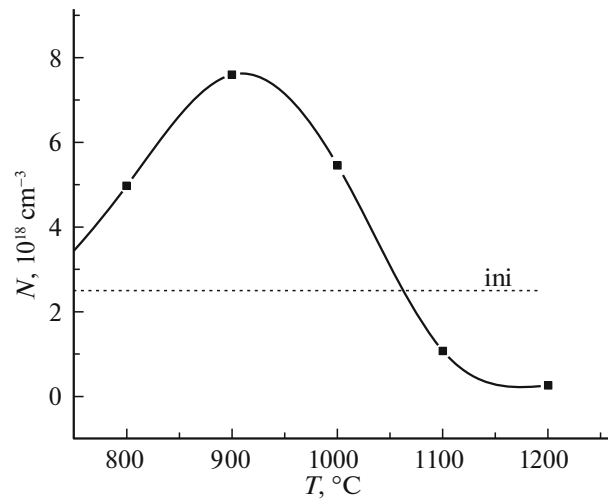
tural units $Si(Si_{4-y}O_y)$ with $y = 1-3$ in the matrix of amorphous SiO, ensures the appearance of numerous nucleation centers. However, these centers have narrow, weakly overlapping fields of collection of migrating Si atoms. Raising the temperature further, which makes faster the diffusion-related mass transfer and enables the reverse transitions of silicon atoms from precipitates to the growth medium, creates more favorable conditions for overgrowth of the coarsest precipitates via the dissolution of finer precipitates. In the process, the distance between the phase-precipitation particles grows. It is important to note that the D/L ratio grows steadily with increasing temperature in the whole temperature range. This means that the process of SiO disproportionation is continuous, with the extent to which the space is filled by the silicon phase becoming larger.

In parallel with an analysis of the data furnished by X-ray diffraction analysis, electron-microscopic images of SiO samples were processed with ImageJ software [23] for prescribed ranges of the size of crystalline particles (Table 5). It is noteworthy that the average values D_{TEM} and L_{TEM} obtained in this case for silicon precipitates are in rather good agreement with

Table 4. Parameters of silicon crystallites, found from X-ray diffraction data

T, °C	D, nm	V_p, nm³	m_p, 10^{-17} mg	M_{Si}, mg/cm³	N, 10^{18} cm⁻³	v, nm³	L, nm	D/L
ini	3.6	24.4	5.7	142.7	2.5	400	9.1	0.40
800	3.3	18.8	4.4	219.4	5.0	200	7.3	0.45
900	3.5	22.4	5.2	404.7	7.7	129.9	6.3	0.56
1000	4.3	41.6	9.7	532.5	5.5	181.8	7.0	0.61
1100	7.8	248.3	57.9	602.8	1	1000	12.4	0.63
1200	13.4	1259.2	293.4	737	0.3	4000	19.7	0.68

Table 5. Results of processing the TM images

Crystallites	Image in Fig. 2	D_{TEM} range being set, nm	D_{TEM}, nm	L_{TEM}, nm
Si	e	0.5–50	3.8	5.3
Si	f	3–50	13.8	22.5
SiO$_2$	g	0.5–50	2.4	7.5
SiO$_2$	h	0.5–50	1.9	6.2

the values of D and L (Table 4) found from the results of X-ray diffraction analysis.

4.4. Activation Energies of the Processes of Diffusion of Si Atoms in a SiO$_x$ matrix and Recrystallization Energies of Clusters Precipitating in the Matrix

The temperature dependence of the diffusion coefficient is expressed by the Arrhenius formula $D_{Si} = D_{Si0}\exp(-E_a/kT)$. If the growth of Si clusters is considered to be determined exclusively by the rate of the diffusion-related mass transfer, the activation energy E_a of the diffusion of silicon atoms can be found either from the temperature dependences of the diffusion length $L_{Si} = \sqrt{D_{Si}t}$, or from the dependence of the crystallite size D. We consider that the values found for the distances between the crystallites L are proportional to L_{Si}. Then, it follows from the slope ratio of the dependence $\log(L^2) = f(1000/T)$ for $T \geq 1000°C$ (Fig. 12) that $E_{a1} = 1.64$ eV. At the same time, the activation energy E_{a2} obtained from the dependence $\log(D^2 - D_0^2) = f(1000/T)$, where D_0 is the initial crystallite diameter, determined in our case for $T = 800°C$ (Fig. 13), appears to be substantially higher, $E_{a2} =$

2.38 eV. It is noteworthy that the first value, E_{a1}, is closer to the published data (1.1 eV [11], 1.9 eV [15]) and falls within the range 1.3–1.8 eV, obtained in [14].

When the values obtained for the activation energy are compared, it is necessary to keep in mind that the activation energy E_a found on the basis of experimental data is related to the process limiting the rate at which the parameter being analyzed varies. In our case, we considered the range of conditions ($T > 900°C$) in which the nucleation of silicon precipitates gives way to their concurrent growth. The quantity L characterizes only the effective size of the region from which migrating Si atoms are collected by a growing crystallite, irrespective of their origin (dissociating amorphous matrix or the previously formed precipitate). At the same time, the change in the average crystallite size $D(T)$ presumes activation of the reverse transition of atoms from the crystalline Si phase to the amorphous SiO$_x$, from which they are incorporated as a result into the largest precipitates. These precipitates must also possess optimal faceting, which ensures that they have the lowest free surface energy. Then, the changes in the averaged parameters, analyzed by us, reflect various processes: temperature-induced changes in the spatial distribution of phase precipita-
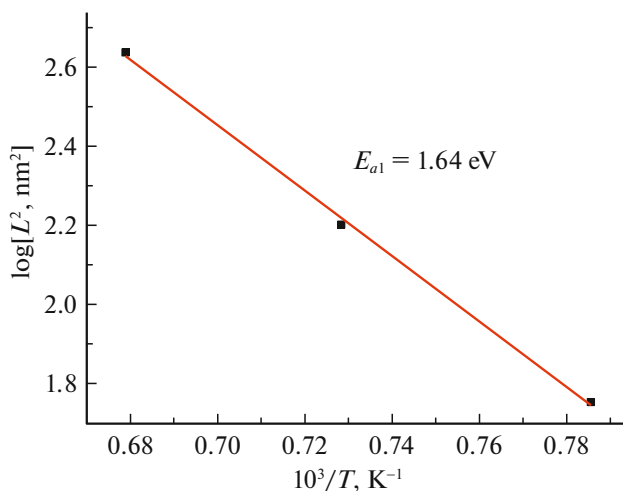

Fig. 12. Dependence of the squared average distance between Si precipitates in the SiO$_x$ matrix on the inverse temperature, determined by the activation energy of Si diffusion in SiO$_x$.
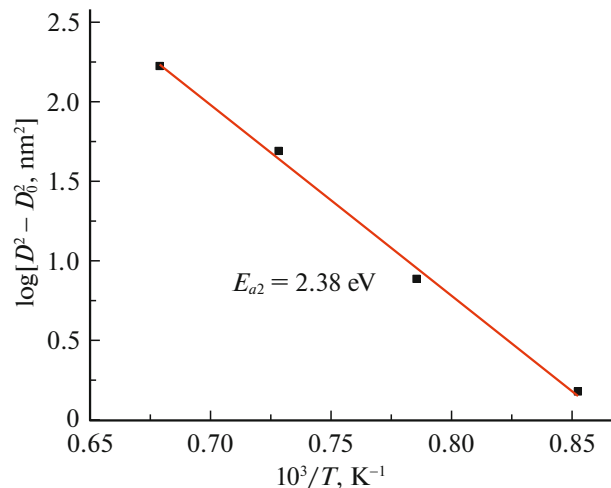

Fig. 13. Temperature dependence of the gain in the squared diameter of Si particles in the SiO$_x$ matrix as a result of isochronous annealing at temperatures exceeding 900°C, determined by the activation energy of Si-atom egress from the precipitate.

tions of silicon upon the isochronous annealing of SiO in the late stages of its disproportionation are largely determined by the activation energy of diffusion of Si atoms in the oxide matrix, whereas changes in the size of competing precipitates are determined by the activation energy of the transition of silicon atoms from the crystalline phase in the surrounding suboxide SiO_x medium. Thus, the value obtained for the activation energy, $E_{a1} = 1.64$ eV, should be related to the process of the diffusion of silicon atoms in an amorphous suboxide of varying composition SiO_x, whereas the value $E_{a2} = 2.38$ eV should be related to the egress of silicon atoms from the crystalline precipitate into the SiO_x medium.

4.5. Anisotropic Deformation of Si Precipitates

Attention should be given to the fact that the peak of the diffraction reflection 111 from small-size Si clusters is shifted in the initial SiO samples to smaller angles relative to the reflection for larger reference silicon particles ($D \approx 40$ nm), for which the peak lies at $2\theta = 28.50°$ (see Fig. 7). Analysis of the decomposition of other Si reflections in the initial material shows that, for the reflections 220 and 400, broad peaks are also shifted relative to the narrow peaks, but now to larger angles, although for reflection 311, to smaller angles, similarly to 111. This is observed in the diffraction patterns for all SiO samples with different amounts of added silicon (see Table 6) and is well seen in Fig. 14.

Table 6 presents the angular positions of the peaks of reflections produced by deconvolution of the diffraction-reflection curves for Si reflections from samples with different concentrations of added free silicon, $2\theta_{av}$ values averaged over three samples, and a shift of the average values for the broad reflections with respect to the narrow reflections, $\Delta 2\theta = 2\theta_{av}(w) - 2\theta_{av}(n)$. The shifts are indicative of the differently directed changes in the interplanar spaces in the lattice of silicon precipitations that exist in the initial SiO relative to the crystal lattice of free silicon particles: the interplanar spaces for the (111) and (311) planes are larger (the lattice is strained), and for (220) and (400) planes, smaller (the lattice is compressed). Here, we believe that the angular positions of the narrow reflections from the added silicon powder correspond to the positions of the diffraction lines associated with the bulk material. Thus, the anisotropy of the elastic deformation appearing in small Si crystallites precipitated from the SiO_x matrix is observed.

Let us trace how the angular positions of the diffraction reflections, interplanar spacings, and the lattice strain vary with increasing annealing temperature and size of Si clusters. Table 7 presents the interplanar spacings d for silicon reflections from d-SiO, calculated by the Wulff–Bragg formula and gives in the lower row the corresponding value for free Si particles

Table 6. Peak positions 2θ of the narrow (n) and wide (w) Si reflections in the diffraction patterns of the initial SiO with the addition of free nanodispersed silicon, found by fitting with the use of Fityk software

Sample→	1.25% Si	2.5% Si	3.75% Si	$2\theta_{av}$, deg	$\Delta 2\theta$, deg
Reflection↓		2θ, deg			
$28n(111)$	28.46	28.53	28.50	28.50	−0.16
$28w(111)$	28.31	28.36	28.35	28.34	
$47n(220)$	47.34	47.41	47.38	47.38	0.10
$47w(220)$	47.50	47.48	47.45	47.48	
$56n(311)$	56.20	56.24	56.20	56.21	−0.32
$56w(311)$	55.83	55.88	55.95	55.89	
$69n(400)$	69.20	69.24	69.20	69.21	0.41
$69w(400)$	69.57	69.67	69.60	69.62	

Table 7. Dependences of the interplanar spacings d in the lattice of Si precipitates for various crystallographic planes on the isochronous-annealing temperature

T, °C	d, Å (111)	d, Å (220)	d, Å (311)	d, Å (400)
ini	3.141	1.913	1.637	1.350
800	3.153	1.912	1.639	1.352
900	3.143	1.909	1.636	1.353
1000	3.142	1.912	1.637	1.353
1100	3.134	1.915	1.636	1.356
1200	3.132	1.917	1.636	1.356
Free Si (40 nm)	3.128	1.917	1.635	1.356

in the nanopowder. It can be seen that, as the annealing temperature increases, d for all four reflections from Si clusters in the SiO_x matrix are shifted toward the values for larger free crystallites. Figure 15 shows how the angular positions of the diffraction reflections of silicon and the relative lattice strains of its precipitates along the corresponding crystallographic directions vary with annealing temperature. For the (111) and (311) planes, the Bragg angles 2θ grow with increasing annealing temperature and, accordingly, $\Delta d/d$ decrease, whereas reverse changes occur for the (220) and (400) planes. However, the angles approach in all cases the value for free Si, and $\Delta d/d$ tend to zero.

It can be seen from these data that the silicon lattice in small precipitates contained in the amorphous matrix is stretched along the diagonal directions and compressed in the direction of the basal planes. Thus, it is impossible to suggest that the deformation of silicon nanocrystals precipitated in the SiO_x matrix is uniform, as assumed by the authors of [14] who traced the position of only a single reflection 111. With increasing annealing temperature and the corresponding increase in the crystallite size, both the deformation and its anisotropy become less pronounced.
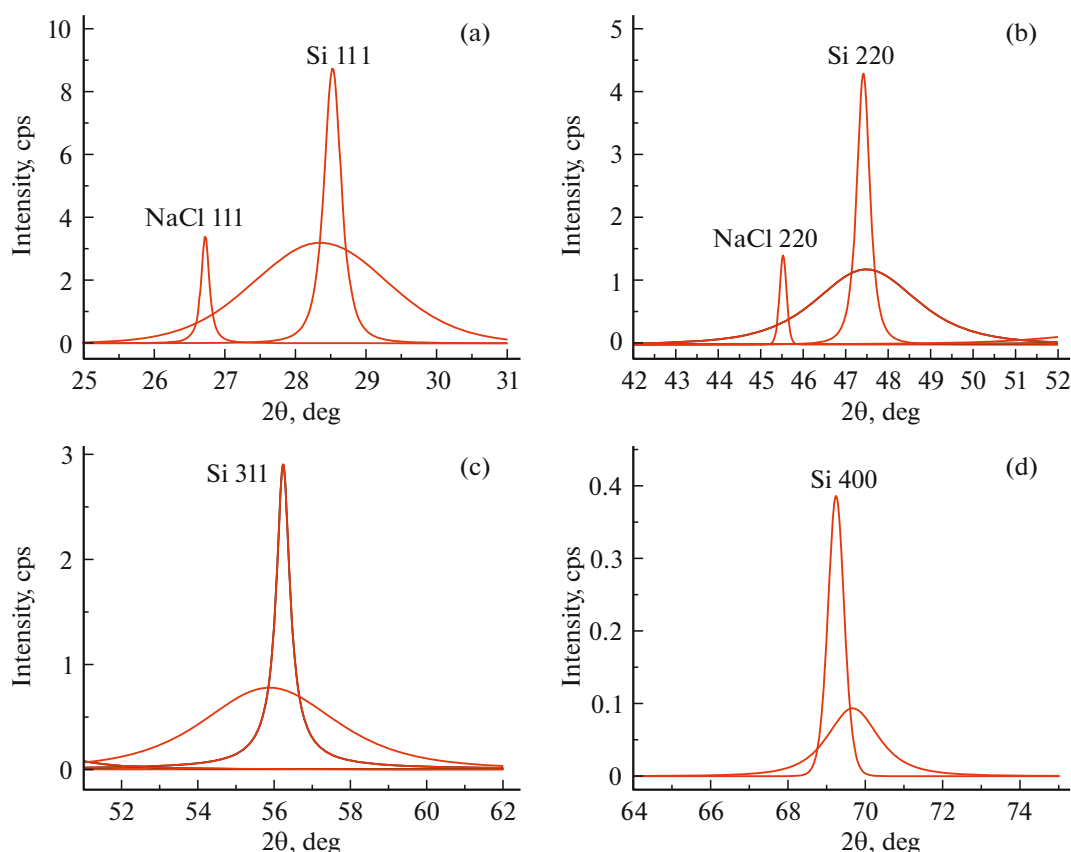
Fig. 14. Decomposition components demonstrating a shift of wide diffraction reflections from Si precipitates in the SiO matrix of the initial material relative to narrow reflections from free silicon nanoparticles for the sample with an addition of 2.5% of Si for the reflections (a) 111, (b) 220, (c) 311, and (d) 400.

The reason why crystalline silicon clusters formed in the solid isotropic amorphous medium of variable composition are deformed can be found in the difference between the specific volumes of crystalline silicon and the conjugated amorphous SiO_x phase that is enriched with silicon dioxide as the medium loses Si atoms. It is known that the length of simple Si–Si and Si–O chemical bonds differ significantly: $l_{Si–Si} = 0.235$ nm and $l_{Si–O} = 0.162$ nm. This means that the packing of the asymmetric mixed structural units $Si(Si_{4-y}O_y)$, interconnected in the SiO bulk is, in principle, more imperfect (having ruptured bonds)

and less dense than the packing of $Si(Si_4)$ units in silicon crystals and $Si(O_4)$ units in the crystal lattices of SiO_2 and even in the structure of quartz glass. Table 8 presents the densities ρ and molar volumes of the possible final phases appearing in the disproportionation of SiO, calculated per gram-atom of a substance, $V_{at} = M/n\rho$ (M is the molar mass, and n is the number of atoms per formula unit), and also relative changes in the occupied volume, $\Delta V_{at} = \{[V_{at}(i) - V_{at}(SiO)]/V_{at}(SiO)\} \times 100\%$ as a result of their separation. It can be seen that silicon atoms occupy upon crystallization a substantially larger volume, compared with the same number of Si and O atoms in the initial amorphous SiO. The remaining atoms are grouped into SiO_4 units that tend to be more closely packed with increasing annealing temperature.

Consequently, the silicon precipitate formed in the course of crystallization must experience in growth directions a compressing deformation caused by the parent phase. This deformation is partly compensated for by the intrinsic compression of the parent phase with increasing concentration in it of more compact SiO_4 structural units and their closer packing. It is important in this case that the surface of the growing

Table 8. Molar volume per gram-atom of a substance and change in the volume relative to SiO

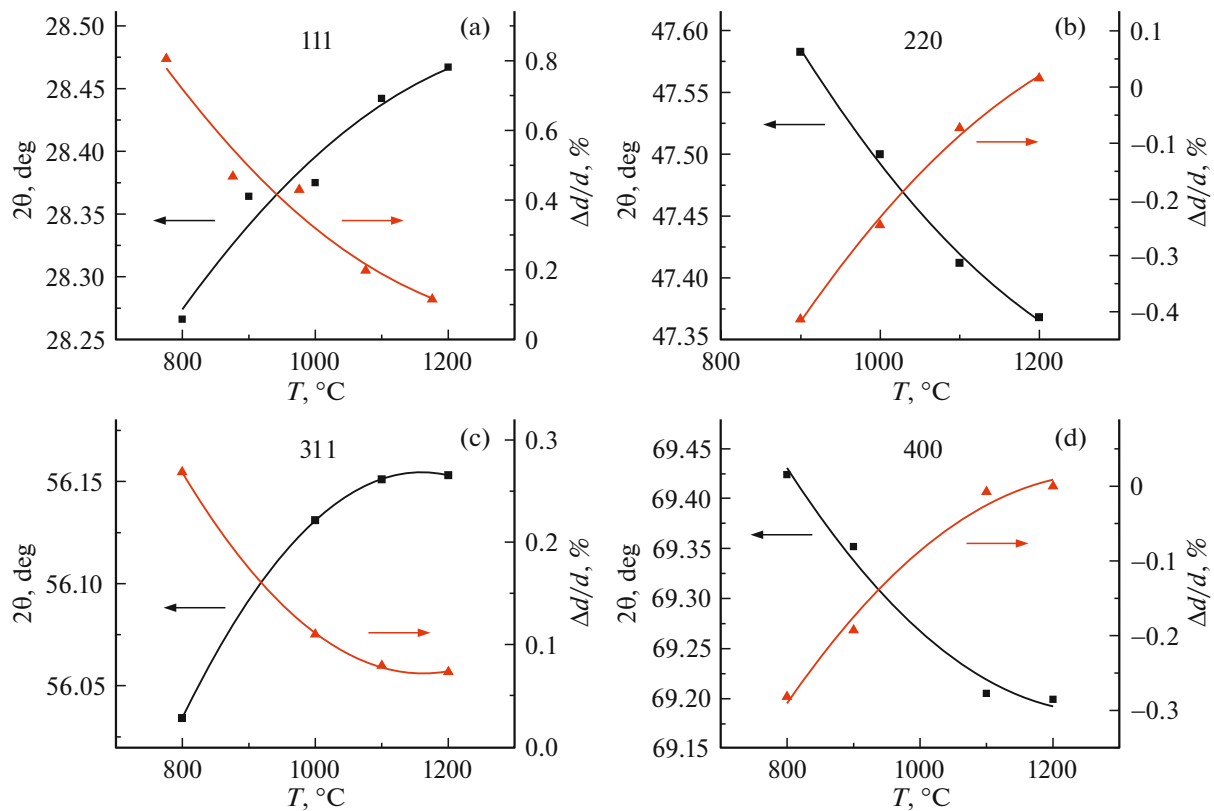| Substance	ρ, g/cm³	V_{at}, cm³/g-atom	ΔV_{at}, %
SiO	2.13	10.329	–
Si	2.33	12.017	16.34
SiO_2, crystalline quartz	2.65	7.547	−26.93
SiO_2, cristobalite	2.34	8.547	−17.25
SiO_2, quartz glass	2.21	9.050	−12.38

Fig. 15. Angular positions of the peaks and relative changes in the interplanar spacings $\Delta d/d$ for silicon reflections (a) 111, (b) 220, (c) 311, and (d) 400 in relation to the SiO annealing temperature.

silicon crystal at least partly preserves =Si−O−Si− chemical bonds with the continuum of bonds in the oxide matrix. In this case, a strong influence on the

Fig. 16. Faceting of the Si precipitate: HRTEM image of the sample annealed at $T = 1225°C$.

type of deformation of a crystal can be exerted by the occurrence of its faceting.

The TEM images of the silicon precipitates in the SiO$_x$ matrix, obtained in the study, do demonstrate that crystallites tend to be faceted by closely packed (111) planes (see the example in Fig. 16, where a silicon nanocrystal is shown in the projection along the axis of a ⟨110⟩ zone). These planes have the smallest number per unit area of potentially possible bonds with the SiO$_x$ growth medium. Accordingly, Si atoms diffusing within this medium reach these planes with the lowest probability. At the same time, having the maximum possible mobility, arriving silicon adatoms tend to be recorded at planes neighboring (111) and at lattice sites with a large number of bonds. Therefore, the highest growth rates are observed for the directions of the ⟨100⟩ type and the same directions become the strongest-compression directions. As a response to anisotropic compression along the directions ⟨100⟩, the interplanar spacings in the directions ⟨111⟩ effectively increase. As the size of the precipitates grows, the contribution to their crystal habit from the (111) planes with the minimum rate of normal growth must become more pronounced. At the same time, the effective internal compression of the SiO$_x$ medium losing silicon atoms must become stronger, which leads to its detachment at least from the surface of the
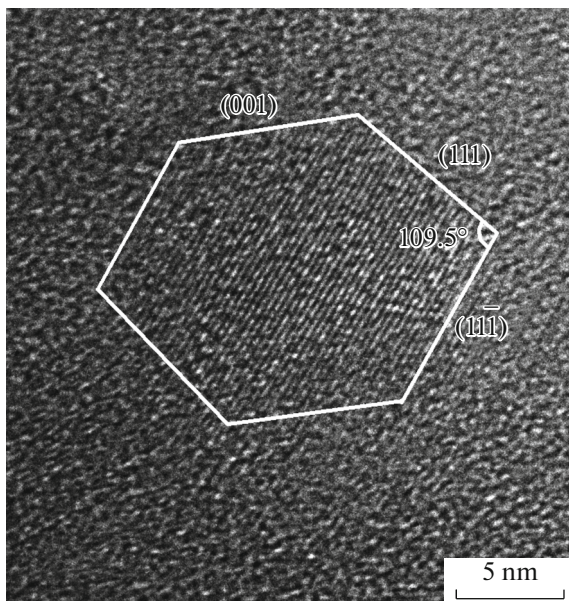
(111) faces. As a result, the cohesion of the precipitates with the growth medium becomes weaker. This, in turn, reduces the resistance to the development of plastic deformation in the strained regions of the amorphous SiO_x mass surrounding the growing crystallites, with the structure of this mass approaching that of the quartz glass in the course of its depletion of silicon. A consequence of the "spreading" of SiO_x along the surface of the precipitates is that the pressure on these from the medium equalizes over the whole phase boundary and the anisotropic deformation disappears. The above-described effects are manifested more clearly, the higher the annealing temperature. (The annealing temperatures used in the study are sufficiently high for activating a viscous flow in the bulk of strained SiO_2 glasses.)

5. CONCLUSIONS

—An excessive amount of silicon was found in the initial SiO amorphous material in the form of nanocrystals with an average diameter of 3.6 nm. The content of the primary silicon precipitates is ~6.7% relative to the total mass of the thermally untreated material.

—The concentration of the precipitated crystalline silicon in the material under study steadily grows with increasing temperature of isochronous (1 h) annealing and reaches ~35% at a temperature of 1200°C, with the ratio of oxygen to silicon in the SiO_x medium surrounding the silicon precipitates increasing to $x = 1.8$.

—The temperature ranges of two fundamentally different stages of formation of crystalline silicon precipitates in the medium of amorphous silicon monoxide are established: nucleation and concurrent growth of the nuclei that appeared. Below $T \approx 900$°C, the nucleation process is dominant, limited by the diffusion rate of atoms in the amorphous matrix. Above this temperature, the dominant process is that in which silicon atoms are transferred between the nuclei that appeared, limited by the egress of its atoms from the crystal lattice into the surrounding SiO_x medium.

—The dependences of the average distance between the precipitates and their averaged diameter on the annealing temperature were used to determine the activation energies of the processes controlling the variation in these parameters: $E_{a1} = 1.64$ eV, associated with the diffusion transport of Si atoms in the amorphous suboxide SiO_x, and $E_{a2} = 2.38$ eV, related to the reverse transition of silicon atoms from the precipitated nanocrystals into the surrounding oxide medium.

—It was found that there is anisotropic deformation of the crystal lattice of the silicon precipitates crystallizing in the solid amorphous medium of SiO_x.

The changes in the interplanar spacings have different signs in the directions [100] (compression) and [111] (strain) and may reach a value of ~0.8%. Raising the annealing temperature leads to a steady decrease in the lattice deformation and its almost complete relaxation at 1200°C. This effect is attributed to the difference between the specific volumes of the initial silicon monoxide and products of its disproportionation, to the anisotropy of the growth rate of the precipitating silicon crystallites, and also to the rise in the plasticity of the SiO_x amorphous medium with increasing annealing temperature.

—In the temperature range under study of SiO disproportionation, the crystallization of silicon dioxide is hindered to such an extent that the density and size of SiO_2 nanocrystals found in the initial material remain nearly invariable. Nevertheless, the shape and the angular position of broad diffraction peaks of the amorphous SiO_x matrix vary with annealing temperature and approach values inherent in cristobalite. Aside from that, additional precipitations of tridymite are observed upon high-temperature annealing (1225°C).

CONFLICT OF INTEREST

The authors state that they have no conflict of interest.

REFERENCES

1. L. Pavesi and D. J. Lockwood, *Silicon Photonics* (Springer, Berlin, 2004).
2. U. Kahler and H. Hofmeister, Appl. Phys. A **74**, 13 (2002).
3. Z. Liu, Q. Yu, Yu. Zhao, R. He, M. Xu, Sh. Feng, Sh. Li, L. Zhou, and L. Mai, Chem. Soc. Rev. **48**, 285 (2019).
4. U. Schubert and T. Weider, in *Silicon Chemistry*, Ed. by P. Jutzi and U. Schubert (Wiley-VCH, Weinheim, 2003), Chap. 18.
5. H. Hofmeister and U. Kahler, in *Silicon Chemistry*, Ed. by P. Jutzi and U. Schubert (Wiley-VCH, Weinheim, 2003), Chap. 19.
6. G. W. Brady, J. Phys. Chem. **63**, 1119 (1959).
7. R. J. Temkin, J. Non-Cryst. Solids **17**, 215 (1975).
8. H. R. Philipp, J. Phys. Chem. **32**, 1935 (1971).
9. A. Hohl, T. Wieder, P. A. van Aken, T. E. Weirich, G. Denninger, M. Vidal, S. Oswald, C. Deneke,

J. Mayer, and H. Fuess, J. Non-Cryst. Solids **320**, 255 (2003).

10. A. Hirata, S. Kohara, T. Asada, M. Arao, C. Yogi, H. Imai, Y. Tan, T. Fujita, and M. Chen, Nat. Commun. **7**, 11591 (2016).

11. M. Mamiya, H. Takeia, M. Kikuchi, and C. Uyeda, J. Cryst. Growth **229**, 457 (2001).

12. M. Mamiya, M. Kikuchi, and H. Takei, J. Cryst. Growth **23**, 1909 (2002).

13. *Silicon Chemistry*, Ed. by P. Jutzi and U. Schubert (Wiley-VCH, Weinheim, 2003).

14. D. Comedi, O. H. Zalloum, E. A. Irving, J. Wojcik, T. Roschuk, M. J. Flynn, and P. Mascher, J. Appl. Phys. **99**, 023518 (2006).

15. L. A. Nesbit, Appl. Phys. Lett. **46**, 38 (1985).

16. S. Gates-Rector and T. Blanton, Powder Diffract. **34**, 1 (2019).

17. S. Gražulis, A. Daškevič, A. Merkys, D. Chateigner, L. Lutterotti, M. Quirós, N. R. Serebryanaya, P. Moeck, R. T. Downs, and A. le Bail, Nucl. Acids Res. **40**, D420 (2012).

18. C.-M. Park, W. Choi, Y. Hwa, J.-H. Kim, G. Jeong, and H.-J. Sohn, J. Mater. Chem. **20**, 4854 (2010).

19. T. Tan, P.-K. Lee, and D. Y. W. Yu, J. Electrochem. Soc. **166**, A5210 (2019).

20. J. Yang, Y. Takeda, N. Imanishi, C. Capiglia, J. Y. Xie, and O. Yamamoto, Solid State Ionics **152−153**, 125 (2002).

21. B. Ding, H. Xuanning, C. Zhenfei, M. Yangzhoua, S. Guangshenga, Y. Weidong, and W. Cuie, Inorg. Chem. Commun. **113**, 107771 (2020).

22. M. Wojdyr, J. Appl. Crystallogr. **43**, 1126 (2010).

23. T. J. Collins, BioTechniques **43**, S25 (2007).

Translated by M. Tagirdzhanov